Arabian Journal of Chemistry (2022) **15**, 104195

King Saud University

Arabian Journal of Chemistry

www.ksu.edu.sa
www.sciencedirect.com

ORIGINAL ARTICLE

Screening of anti-inflammatory and antioxidant potential of functionalized tetrahydrocarbazole linked 1,2-diazoles and their docking studies

Ambreen Ghani [a], Zubi Sadiq [b], Sadaf Iqbal [c], Abida Yasmeen [b], Shahida Shujaat [b], Iftikhar Ali [d,*]

[a] *Department of Chemistry, University of Education Lahore, Vehari campus, Pakistan*
[b] *Department of Chemistry, Lahore College for Women University, Lahore, Pakistan*
[c] *Department of Chemistry, University of Karachi, Pakistan*
[d] *Department of Chemistry, Karakoram International University, Gilgit 15100, Pakistan*

Received 7 May 2022; accepted 9 August 2022
Available online 12 August 2022

KEYWORDS

Diazoles;
Toxicity;
Human red blood cells membrane stabilization;
Anti-inflammatory agents;
Lipid peroxidation;
Simulation study

Abstract Inflammatory diseases are associated with life-threatening syndromes like hepatitis, cancer, and trauma injury while some decrease the quality of life such as rheumatism, arthritis, and tuberculosis. 1,2-Diazoles (pyrazolines) play a vital role in COX-2 inhibition thus dinitro-tetrahydrocarbazole linked pyrazolines have been synthesized and endeavor to screen for anti-inflammatory, antioxidant and molecular docking studies. For this purpose, 6,8-dinitro-acetyl-2,3 ,4,9-tetrahydrocarbazole (I), aromatic aldehydes (IIa-e) and hydrazines (IIIa-b) were combined via multicomponent reaction approach under the influence of microwave irradiations to afford pyrazolines (1–10). All new molecules were screened for *in vitro* anti-inflammatory activity by human red blood cells membrane stabilization, antioxidant potential by2,2-diphenyl-1-picrylhydr azyl,2,2′-azinobis (3-ethylbenzo thiazoline)-6-sulphonic acid, lipid peroxidation, and total antioxidant capacity assays along with cytotoxicity by brine shrimp lethality assay. Molecular docking was performed by using the Auto Dock program. Both disubstituted and trisubstituted diazoles showed excellent membrane stabilizing effects, (91.89 % and 77 %, respectively). The presence of phenol, furan, thiocarbamide, and chloro-moieties have the most prominent effect. Toxicity results indicated that compounds were less toxic at the tested dose (0.1 mg/ml). The antioxidant study showed that compound **2** was more active showing low IC_{50} values (32.2 and 39.2 μg/ml) in DPPH and total phenolic contents assays respectively. Compound **3** (44.0 μg/ml) showed the highest

* Corresponding author at: Department of Chemistry, Karakoram International University, Gilgit 15100, Pakistan.
E-mail addresses: ambreen.ghani@ue.edu.pk (A. Ghani), Abida.Yasmeen@lcwu.edu.pk (A. Yasmeen), iftikhar.ali@kiu.edu.pk (I. Ali).
Peer review under responsibility of King Saud University.

Production and hosting by Elsevier

https://doi.org/10.1016/j.arabjc.2022.104195

potential assay in ABTS radical neutralization assay while compound **7** (65.0 μg/ml) showed maximum potential in lipid peroxidation. All diazoles (**1**–**10**) were screened for *in vitro* anti-inflammatory potential where disubstituted diazoles were found better than trisubstituted analogs and exhibited significant antioxidant potential. Molecular docking of diazoles showed a good correlation of their anti-inflammatory activity with p38α MAPK, COX-2, and 5-LOX enzymes that are molecular therapeutic targets of inflammation.

1. Introduction

1,2-Diazole such as pyrazoline has occupied a prominent position in the field of medicinal chemistry. Pyrazolines consist of five member heterocyclic ring having two adjacent nitrogen atoms with an endocyclic double bond (Thach et al., 2021). It is the core nucleus of COX-2 inhibitor, Celecoxib and other anti-inflammatory drugs (Fig. 1). Among several methods available for the synthesis of this bioactive molecule, multicomponent reaction is the most popular. This method is even more effective when proceeded by using microwave energy. The synergistic effect of these two resulted in a neat reaction in lesser time and higher yield.

Inflammation is the natural procedure adopted by the body in response to any damage. The repeated inflammation resulted in tissue destruction and fibrosis (Kostopoulou et al., 2021). This in turn led to various diseases which decrease life quality and commonly include degenerative diseases like diabetes, cancer, rheumatoid arthritis, and bowel diseases (Prasad et al., 2021, Oyedapo and Famurewa 1995). Among many important enzymes, pro-inflammatory enzymes, Cyclooxygenase (COX), and lipoxygenase (LOX) enzymes play a key role in producing inflammatory mediators' prostaglandins (PGs) *via* arachidonic acid (a polyunsaturated fatty acid present in the cell membrane) pathway. COX-2 expression is rapidly induced by stimuli such as proinflammatory cytokines (IL-1β, TNFα), and disorders of water-electrolyte hemostasis, resulting in increased synthesis of PGs in inflamed and neoplastic tissues. Thus, COX-2 has been implicated in pathological processes such as inflammation and various cancer types (Williams and DuBois 1996, Konturek et al., 2005). Lipoxygenase enzymes belong to a class of non-heme iron-containing enzymes that catalyze the hydro-peroxidation reaction of fatty acids including arachidonic acid to peroxides (Gilbert et al., 2021). Lipoxygenases exist in three isoforms, lipoxygenase-5, lipoxygenase-12, and lipoxygenase-15. Among them, LOX-5 is involved in the production of leukotrienes, which are known to contribute to the progression of osteoarthritis, asthma, and inflammation (Watterson et al., 2013). Mitogen-activated protein kinases (MAPK) are a family of proline-directed Serine/threonine kinases, which are activated by a variety of signals including nutritional and osmotic stress, UV light, growth factors, endotoxin, and inflammatory cytokines. The p38 MAP kinase group consists of four isoforms including p38α, p38β, p38γ, and p38δ, and is responsible for phosphorylating and activating transcription factors (e.g. ATF2, CHOP, and MEF2C) as well as other kinases (e.g. MAPKAP-2 and MAPKAP-3). The isoform p38αinduces the transcription of COX-2 and its inhibition results in the down-regulation of COX-2 expression and PG-E2 production (Kurumbail et al., 1996, Limongelli et al., 2010). It is also an important mediator of inflammatory cytokines including TNF-α and IL-1β (Nieminen et al., 2005, Schieven 2005, Amir et al., 2013). Moreover, numerous preclinical studies demonstrated that inhibition of p38α MAPK could effectively inhibit TNF-α production *in-vitro* and *in-vivo* (Kumar et al., 2003, Saklatvala 2004, Natarajan et al., 2006). anti-inflammatory agents block the synthesis of prostaglandin by either inhibiting the COX-2 enzyme or protecting the lysosomal membrane from breakdown. Since human red blood cell (HRBC) membranes are similar to these lysosomal membrane components, the prevention of hypotonicity induced HRBC.

. Lysosomal enzymes have an imperative role in the advancement of severe and prolonged inflammation. Due to structural similarities with human red blood cells, the membrane stabilization method can be employed to determine inflammatory responses to natural or synthetic compounds (Liu et al., 2005). When the HRBC membrane is ruptured, the cell will be vulnerable to damage through free radical-induced lipid peroxidation (Revesz et al., 2004). Since the use of acetylsalicylic acid, many steroidal and non-steroidal anti-inflammatory drugs (NSAIDs) are beneficial along with severe side effects. These adverse effects have led researchers to explore more benign anti-inflammatory agents. Diazoles are potential candidates, which exhibit an anti-inflammatory effect (Mehmood et al., 2022). The molecular architecture of diazole is functionalized to get structural diversity, in this connection, tetrahydrocarbazole coupled diazoles were synthesized *via* pot atom simple economy (PASE) approach in the synthetic microwave and compared with reflux heating in the presence of aqueous-Brønsted acid catalytic system (Ashour and Khateeb 2011, Wu et al., 2012).

After achieving successful synthesis and structure confirmation of diazoles (Sadiq et al., 2017), the present study aims to assess their biological potential via *in-vitro* anti-inflammatory assay along with cytotoxicity and antioxidant assay, and ten derivatives of diazoles (**1**–**10**) (Fig. 1) were found active.

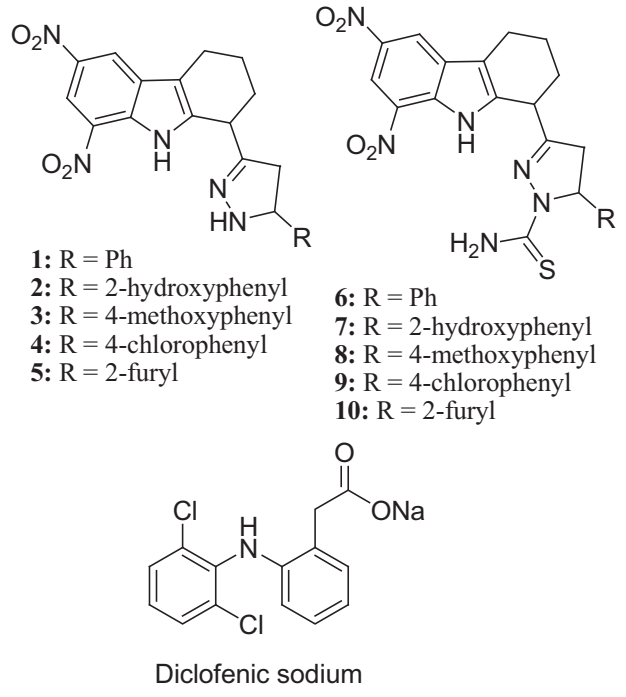

Fig. 1 Tetrahydrocarbazole linked 1,2-Diazoles (**1**–**10**) and Standard drug.

2. Materials and methods

2.1. Chemicals and instruments

All chemicals used for the analysis were analytical grade. Standard drugs diclofenac sodium, Trolox, ascorbic acid, and propyl gallate were used for different experiments purchased from Sigma. UV/Visible spectrophotometer was used to measure the absorption in all *in vitro* experiments.

2.2. Human red blood cells membrane stabilization method

Healthy human volunteers who had not received any NSAIDS for two weeks donated blood (HRBCs) used for the experiments (Karrat et al., (2022)). An equal volume of blood and Alsever solution (2% dextrose, 0.8% sodium citrate, 0.5% citric acid, and 0.42% sodium chloride in distilled water) were mixed in heparinized tubes followed by 10 min centrifuge at 4000 rpm. The erythrocytes were obtained after discarding the supernatant layer, to afford 10% *v*/*v* suspension it was washed with isosaline solution and stored at 4°C. Compounds (**1**–**10**) and standard (diclofenac sodium) were prepared in dimethylforamide at different concentrations of 100, 10, 1, and 0.1 µg/mL. In centrifuge tubes, hyposaline (2 mL), phosphate buffer (1 mL), test sample (1 mL), and 0.5 mL of erythrocyte suspension were mixed. The control was prepared in distilled water for complete hemolysis. All these tubes were incubated at 37°C for half an hour and centrifuged at 4000 rpm for ten minutes. The hemoglobin contents of the supernatant solution were estimated by spectrophotometer at 560 nm. The formula for calculating the percentage of HRBC membrane stabilization is given as:

$$Percentage Stabilization = (Absorbance of control - Absorbance of Test)/100$$

Brine shrimps lethality assay.

Well-known brine shrimps lethality assay was used to evaluate the toxicity of compounds (**1**–**10**). The Brine shrimps eggs were hatched in artificial seawater (5.7 g of sea salt in 1000 mL distilled water) to get larvae (Anosike et al., 2012). In semi-translucent hatching cone brine shrimp eggs having seawater, a pinch of baking soda was taken, and the continuous supply of oxygen was maintained with the help of an air pump. The eggs were hatched for approximately 24 h. A stock solution of each compound was diluted to get different concentrations ranging from 1 to 0.1 mg/mL. An equal volume of all compounds and seawater containing 30 nauplii was kept overnight at room temperature. After 24 h, dead larvae were counted with the help of magnifying glass. DMSO and distilled water were used as control. Percentage mortality was calculated using the formula:

Percentage of death = (Total nauplii – Alive nauplii) × 100 / Total nauplii.

2.3. Antioxidant assays

2.3.1. DPPH radical scavenging assay

All synthesized compounds were screened for their 1,1-diphenyl-2-picrylhydrazyl (DPPH) assay free radical scavenging capacity with minor modification in the reported method (Kumar et al., 2011, Sadiq et al., 2017). Different concentrations of analytes (**1**–**10**) (0.5 mL) and DPPH solution (2.5 mL) in methanol were prepared to afford a final concentration of 0.1 mM. The mixture was homogenized, incubated at 37°C for thirty minutes and absorbance was observed at 517 nm using a UV/Visible spectrophotometer. Radical scavenging percent was calculated as:

% Inhibition = [1-Absorbance$_{(sample)}$/ Absorbance$_{(control)}$] × 100.

2.3.2. $ABTS^{\bullet+}$ decolourization assay

The solution of 2, 2′-azinobis (3-ethylbenzo thiazoline)-6-sulphonic acid ($ABTS^{\bullet+}$) decolorization ability of compounds (**1**–**10**) and Trolox as standard was evaluated by the reported method (Prieto et al., 1999). 7.0 mM ABTS stock solution was oxidized by 2.45 mM $K_2S_2O_4$ to generate ABTS radical cation. The absorption of the resultant solution was adjusted up to 0.70 ± 0.10 at 734 nm. The reaction mixture contained 2.5 mL $ABTS^{\bullet+}$ and 0.5 mL compound solution was incubated at room temperature for 5 min and percentage quenching was estimated. The following equation is used for calculating the antioxidant index for ABTS, lipid peroxidation and TAC.

% Inhibition = [1-Absorbance $_{(sample)}$/ Absorbance $_{(control)}$] × 100.

2.3.3. Lipid peroxidation assay

A modified Halliwell *et al.* method was used to estimate the lipid peroxidation activity of samples and standards (Halliwell 2007, Sherin et al., 2015). In brief, 1.15% KCl (1.5 mL) and 10.0% egg yolk (1.0 mL) were added to samples followed by the addition of 0.5 mL of 0.2 mM ferric chloride and the mixture was incubated for 1 h at 37°C. The reaction was then ceased by adding 2 mL of ice-cold HCl (0.25 N) containing 0.38 % thiobarbituric acid (TBA), 15.0% trichloroacetic acid and 0.5% butylated hydroxytoluene. It was heated for an hour at 80°C, followed by centrifugation at 3000 rpm, and measured by spectrophotometer at 532 nm.

2.3.4. Total antioxidant capacity

To determine the total antioxidant capacity of diazoles (**1**–**10**), 0.5 mL of each compound was added to 4 mL of reagent solution (0.6 M sulfuric acid, 28 mM sodium phosphate, and 4 mM ammonium molybdate), incubated for 90 min at 95°C and absorbance was measured at 695 nm with a spectrophotometer. The control experiment was performed in methanol only using ascorbic acid as standard (Re et al., 1999).

2.4. Molecular docking

The 3D structures of all synthetic diazoles were modeled and minimized using ArgusLab (Lugasi 1997) with the semi-empirical (AM1) parameterization (Parke 1991). The energy minimization was performed by the Restricted Hartree-Fock (RHF) closed-shell method. Maximum iterations were set to 200 and geometry search gradient conversion was 10^{-1} Kcal/-mol/Å. The synthetic diazoles modeled and energy minimized structures were further modified for docking by merging polar hydrogen atoms, adding Gasteiger partial charges, and defining rotatable bonds using AutoDock Tools. All bound ligands and water molecules were deleted to prepare all protein structures for docking. Polar hydrogen atoms and Kollman united

atom charges were added using AutoDock Tools (Prieto et al., 1999). The structures were saved in PDBQT file format where the center of the box was set at the co-crystallized ligand and grid energy calculations were carried out. Docking calculations were performed with AutoDock Vina using the Lamarckian Genetic Algorithm (Thompson 2004). Twenty docked conformations were generated for each compound. The energy of the binding interactions was estimated using a genetic algorithm. The outputs were exported to CHIMERA for visualization of the binding modes in the active sites (Dewar et al., 1985).

2.4.1. Cox-2

The crystal structure of human cyclooxygenase-2 (COX2) in complex with SC-558 was fetched from the PDB using ID: 1CX2 with 2.50 Å resolutions (Trott and Olson 2010). Around the binding site of the co-crystallized ligand, a grid box with the dimension of $26 \times 26 \times 26$ Å^3 with 1 Å spacing centered on 21.583, −3.655, 36.436 was created using ADT.

2.4.2. 5-Lox

The crystal structure of S663D mutant human lipoxygenase (5-LOX) in complex with arachidonic acid was fetched from the PDB using ID: 3V99 with 2.25 Å resolutions (Morris et al., 1998). A grid box size of $25 \times 25 \times 25$ Å^3 points with a grid spacing of 1 Å was generated using AutoGrid. The grid was centered at x, y, and z coordinates of 16.317, −78.717, and –32.292, respectively, which were reported as the binding site residues of arachidonic acid.

2.4.3. MAPK p38α

The crystal structure of human p38α MAPK in complex with novel and selective inhibitor [N,*N*-dimethyl-6-(naphthalen-2-yl)-5-(pyridin-4-yl)pyridazin-3-amine] was retrieved from the PDB having ID: 4F9W with 2.00 Å resolutions (Pettersen et al., 2004). Around the binding site of the co-crystallized ligand, a grid box with the dimension of $25 \times 25 \times 25$ Å^3 with 1 Å spacing centered at x, y, and z coordinates of −2.149, 0.938, 21.764, respectively, was created using ADT. AutoDock parameter were set and distance-dependent dielectric functions were used for calculating the van der Waals and the electrostatic terms, respectively. The docked conformations of diazole derivatives were derived from 100 independent docking runs that were set to terminate after a maximum of 2.5×10^6 energy evaluations with a mutation rate of 0.02 and a crossover rate of 0.8.

2.4.4. Statistical analysis

Statistically, the data were analyzed by using ANOVA (SPSS version 20) as mean ± standard deviation, while P values < 0.05 were considered significant. IC_{50} values were calculated by plotting a graph between concentrations versus percentage stabilization values using Graph Pad Prism software version 6.07.

3. Results and discussion

3.1. Chemistry

One pot multicomponent synthetic strategy under microwave energy was adopted for the synthesis of 1,2-diazoles also known as pyrazolines (**1**–**10**) (Scheme 1) and reported in our previous study (Sadiq et al., 2017). The advantage of using microwave resulted in better yield than conventional heating mode with short reaction time and neat reaction. 6,8-Dinitro acetyltetrahydrazole played the role as ketone (**I**), aromatic aldehydes (**IIa-e**) and hydrazines (**IIIa-b**) were reacted together in catalytic influence of acetic acid–water (1:1) when irradiated by synthetic microwave.

3.2. HRBC membrane stabilizationstudies

All synthesized diazoles (**1**–**10**) and standard drug have been evaluated for *in vitro* anti-inflammatory activity by using HRBC membrane stabilization method. Among all the tested compounds, two different types of trends, i.e. with concentration-dependent or independent were observed (Fig. 2). In compounds **1**, **5**, **6**, **9,** and **10** the percent stabilization was found to be inversely proportional to the concentration; these compounds gave minimum stabilization at maximum concentration while compounds **2**, **3**, **4**, **7,** and **8** showed a direct relationship. The anti-inflammatory potential is governed by the substituent present in diazoles. Compound **1** showed 61.44% membrane stabilization at minimum concentration, while at maximum concentration 43% stabilization was observed. Phenol moiety in compound **2** exhibited maximum membrane stabilization among all the disubstituted compounds tested (77.6%) at 100 ppm, the percentage stabilization reduced with a decrease in the concentration, and 55% stabilization was observed at 0.1 ppm.

Compound **3** having methoxy group present on phenyl group attached to the diazole ring also revealed a concentration-dependent mode with 76.4% membrane stabilization potential at 100 ppm. Compound **4** having chloro group at phenyl on diazole ring expressed concentration-dependent behavior, which is amplified with an increase in concentration. The maximum of 69.9% potential was observed at 100 ppm. The presence of furan substituent at C-3 of diazole in compound **5** led to 77%, the second-highest membrane stabilization at 0.1 μg/mL, which describes the inverse relationship between activity and concentration. In trisubstituted diazoles, derivative **6** having N-substituted thiocarbamide in the diazole ring showed somewhat diminished activity at the highest concentration (100 ppm) but revealed concentration-independent behavior for percentage stabilization of erythrocyte membrane with maximum 40% activity at minimum concentration. Compound **7** also has a concentration-dependent mode showing 74.5% activity at maximum concentration and 70% at minimum concentration i.e. 0.1 ppm. Compound **8** possessing methoxy substituent in diazole revealed concentration-dependent behavior with 46% activity at 100 μg/mL, which was almost two folds lesser than the standard drug at the same dilution. Substitution of both thiocarbamide and phenyl having chloro group attached to the diazole ring greatly reduced hypotonicity induced hemolysis of compound **9**. It displayed a dramatic increase in anti-inflammatory activity as compared to the derivatives having thiocarbamide and chloro groups individually. It showed excellent ≃92% activity against an optimum concentration of 0.1 μg/mL and proved more effective with an IC_{50} value of 1.89 μg/mL. At the same concentration, the reference drug revealed only 60% potential against hemolysis of RBCs. Compound **10** revealed this maximum activity at 0.1 μg/mL with an

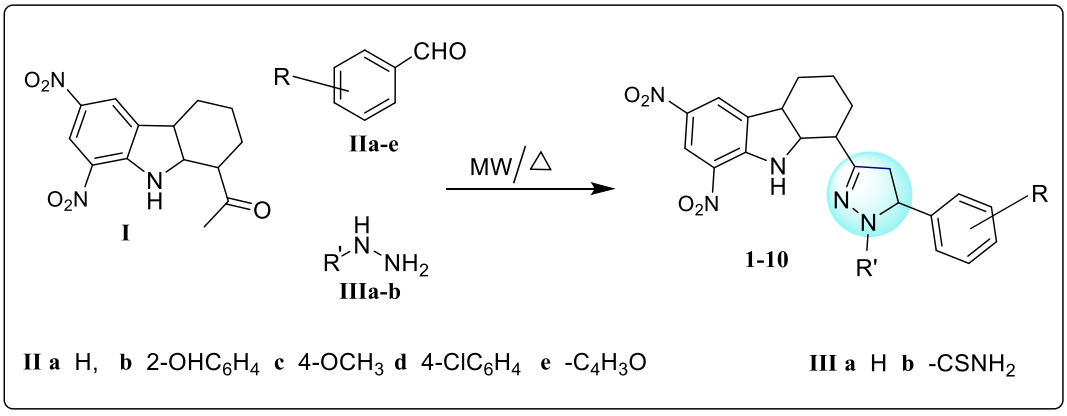

Scheme 1 One pot multicomponent synthetic strategy for the synthesis of 1,2-diazoles.

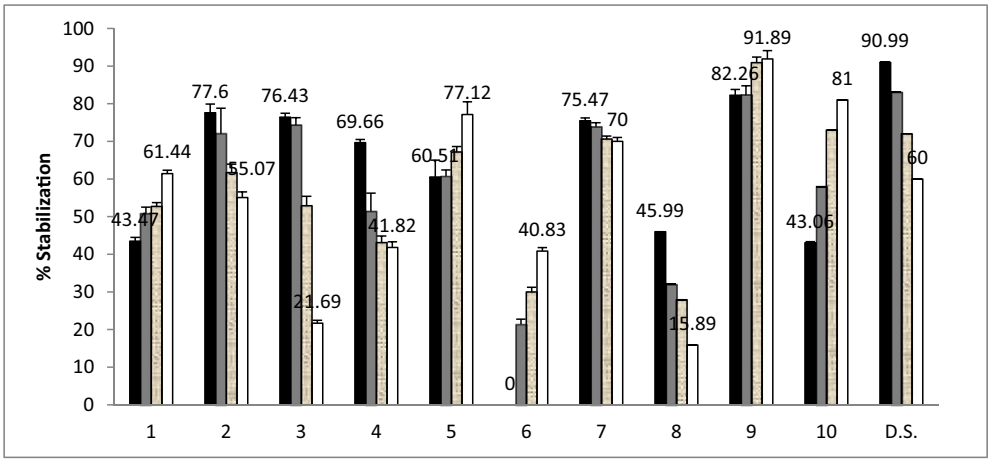

Fig. 2 Effect of membrane stabilization at different concentrations of **1**–**10.**

IC_{50} value of 1.66 µg/mL. The hemolysis was influenced by the presence of both thiocarbamide and furan groups at C-3 of the diazole ring causing the increase of anti-inflammatory potential with 81% protection of membrane (Fig. 2).

3.3. Brine shrimp lethality studies

This efficient and reliable method demonstrated that almost all compounds are relatively less toxic at the lowest concentration (0.1 mg/mL) while toxic at a higher concentration of **1** mg/mL (Table 1).

3.4. Antioxidant studies

3.4.1. DPPH radical scavenging potential

DPPH assay results indicated that all synthetic compounds (**1**–**10**) possess anti-radical potential (Table 2). First, five compounds (**1**–**5**) containing disubstituted diazoles showed better results than trisubstituted diazoles. Among the members of disubstituted diazoles, compound **2** with a phenyl group attached to the diazole ring was more potent (IC_{50} value, 32.2 µg/mL) than others due to the electron-donating —OH group. Compound **4** showed better results (IC_{50} value, 34.0 µg/mL) than **3** and **5** due to the presence of chloro substituent at the phenyl ring attached to the diazole ring. The order of decreasing radical scavenging potential of disubstituted diazoles is **2** > **4** > **1** > **3** > **5**. Trisubstituted diazoles (**6**–**10**) exhibited lower radical scavenging potential as compared to disubstituted diazoles. Among these, compound **7** (IC_{50}, 44.2 µg/mL) containing —OH group on phenyl ring showed improved results and was comparable with compound **5** (IC_{50}, 43.7 µg/mL) among disubstituted diazoles while other compounds showed intermediate potential, **8** > **9** > **6** > **7** > **10**.

3.4.2. ABTS assay

This assay is rapid and sensitive with minimum side reactions where antioxidant compound neutralized ABTS radical cation by donation of the electron. The results agree with the DPPH assay results that, disubstituted diazoles were more active than the tri-substituted series (Table 2). Amongst all compounds (**1**–**10**) the compounds having methoxy group at phenyl attached to the diazole ring were more active (Compound 3; IC_{50}, 44.0 µg/mL) than compounds **1,2, 4,** and **5** and (compound **8**; IC_{50}, 50.20 µg/mL) than **9, 6, 7** and **10**.

3.4.3. Lipid peroxidation assay

In lipid peroxidation assay, peroxy radicals generated by peroxidation of fatty acids decompose into malondialdehyde, this product reacts with thiobarbituric acid TBA, which is mea-

Table 1 Cytotoxicity evaluation of **1**–**10** at 24 h.

Entry	Dilutions (mg/mL)	Mortality (%)	Entry	Dilution (mg/mL)	Mortality (%)
1	1.00	93	**6**	1.00	70
	0.75	73		0.75	56
	0.50	53		0.50	47
	0.10	23		0.10	36
2	1.00	86	**7**	1.00	96
	0.75	66		0.75	83
	0.50	47		0.50	63
	0.10	36		0.10	53
3	1.00	96	**8**	1.00	56
	0.75	70		0.75	43
	0.50	53		0.50	36
	0.10	30		0.10	23
4	1.00	73	**9**	1.00	90
	0.75	53		0.75	76
	0.50	33		0.50	63
	0.10	13		0.10	47
5	1.00	53	**10**	1.00	96
	0.75	47		0.75	76
	0.50	30		0.50	60
	0.10	23		0.10	53

All experiments were performed in triplicate; TD: Total Dead.
Control: DMSO (100% mortality at all test concentrations).

Table 2 Comparison among antioxidant assays of **1**–**10.**

Entry	IC_{50} (μg/mL)				Entry	IC_{50} (μg/mL)			
	DPPH	ABTS	LPO	TAC		DPPH	ABTS	LPO	TAC
1	39.7 ± 0.10	51.0 ± 0.12	66.4 ± 0.20	51.5 ± 0.10	6	46.9 ± 0.08	51.0 ± 0.30	70.4 ± 0.09	55.5 ± 0.08
2	32.2 ± 0.90	45.7 ± 0.07	72.1 ± 0.28	39.2 ± 0.09	7	44.2 ± 0.65	54.2 ± 0.90	65.0 ± 0.99	52.5 ± 1.90
3	40.7 ± 1.00.	44.0 ± 0.80	77.5 ± 0.09	42.0 ± 0.04	8	47.2 ± 0.10	50.2 ± 0.20	74.0 ± 1.00	56.0 ± 0.90
4	34.0 ± 0.09	49.3 ± 0.10	76.0 ± 0.90	44.2 ± 0.02	9	45.0 ± 0.09	58.7 ± 0.15	77.9 ± 0.50	57.3 ± 0.59
5	43.7 ± 0.20	61.5 ± 0.30	68.4 ± 0.80	56.5 ± 0.30	10	50.9 ± 0.30	57.9 ± 0.05	67.6 ± 0.89	60.2 ± 0.87
n-Propyl Gallate	2.31 ± 0.04	1.71 ± 0.03	0.42 ± 0.02	4.54 ± 0.30	Trolox	6.17 ± 0.02	3.86 ± 0.03	0.08 ± 0.02	3.97 ± 0.60

sured to quantify the level of peroxidation LPO 2. During the initial screening, all compounds showed encouraging anti-lipid peroxidation potential inferred by IC_{50} values of compounds **1**–**10** (Table 2). According to the results, compound **7** showed maximum potential (65.0 μg/mL) while compounds **1** and **10** showed almost the same potential IC_{50}, 66.4, and 67.6 μg/mL, respectively revealing better results than the remaining compounds which showed moderate activity.

3.4.4. Total antioxidant capacity

Total antioxidant activity of compounds **1**–**10** was measured at 695 nm by reduction of Mo(VI) to Mo(V). Maximum capacity was revealed by compound **2** (IC_{50}, 39.2 μg/mL) and compound **7** (IC_{50}, 52.2 μg/mL) among all tested compounds (Table 2).

3.5. Molecular docking

Molecular docking of synthesized diazoles was carried out against three anti-inflammatory drug targets (COX-2, 5-LOX, *p38α* MAPK). The binding energy of the ten synthesized diazole derivatives (di-substituted compounds **1**–**5** and tri-substituted compounds **6**–**10**) against three anti-inflammatory drug targets are listed in Table 3. The order of the anti-inflammatory potential of diazoles (Compounds **1**–**10**) from highest to lowest is **2 > 3 > 6 > 5 > 1 > 10 > 9 > 7 > 8 > 4**. According to the measured anti-inflammatory activity, compounds **2** (IC_{50} = 0.06 μg/mL), **3** (IC_{50} = 0.7 μg/mL), **5** (IC_{50} = 0.86 μg/mL) and **6** (IC_{50} = 0.82 μg/mL) showed very strong potential, compounds **1** (IC_{50} = 1.36 μg/mL), **7** (IC_{50} = 2.91 μg/mL), **9** (IC_{50} = 1.8 9 μg/mL) and **10** (IC_{50} = 1.66 μg/mL) illustrated good and comparable potential while compounds **4** (IC_{50} = 28.61 μg/mL) & **8** (IC_{50} = 28.22 μg/mL) demonstrated moderate potential as compared to the standard anti-inflammatory drug, diclofenac (IC_{50} = 7.7 μg/mL). The results of the docking of synthesized diazoles against each anti-inflammatory drug target protein are described in the later sections.

3.5.1. COX-2

The crystal structure of human cyclooxygenase-2 (COX2) in complex with the selective inhibitor SC-558 (PDB-ID: 1CX2) is used to describe the binding mode of diazole derivatives

Table 3 Results of **1**–**10** for their anti-inflammatory potential.

Entry	IC_{50} (μg/mL)	COX-2 binding energy (Kcal/mol)	p38α MAPK binding energy (Kcal/mol)	5-LOX binding energy (Kcal/mol)
1	1.36	−9.2	−9.2	−9.0
2	0.06	−9.4	−10.2	−9.8
3	0.7	−9.3	−9.8	−9.1
4	28.61	−7.4	−8.2	−8.4
5	0.86	−8.9	−9.3	−9.2
6	0.82	−7.1	−9.6	−9.3
7	2.91	−7.3	−8.7	−8.8
8	28.22	−7.6	−8.4	−8.1
9	1.89	−7.2	−8.7	−8.6
10	1.66	−7.4	−8.6	−8.9
Diclofenac sodium	7.7	–	–	–

(Trott and Olson 2010). The COX-2 active site has been suggested to contain three binding regions; common pocket (residues M113, V116, R120, V349, Y355, L359, and L531), cyclooxygenase channel (residues Y348, F381, L384, Y385, W387, G526, A527, and S530), and selectivity pocket (residues H90, N192, L352, S353, R513, A516, I517, F518, and V523). The common pocket is known to occupy also by the aromatic ring of many nonselective COX inhibitors (Gilbert et al., 2021). The selectivity pocket is present at the side of the main cyclooxygenase channel and responsible for the selectivity of "coxibs" for COX-2 (Watterson et al., 2013). Fig. 3A describes the binding of SC-558 into three binding regions such that the trifluoromethyl group attached to the diazole ring of SC-558 is anchored within the common pocket, the bromophenyl ring is enclosed inside the cyclooxygenase channel and the phenylsulphonamide moiety is bound into the selectivity pocket (Fig. 3B). The oxygen atom of the sulphonamide moiety forms a hydrogen bond with R513 and H90 while the amide hydrogens interact with the backbone of F518 through two water bridges.

The synthesized diazole derivatives are found to follow the binding mode of the selective inhibitor SC-558 against COX-2. Fig. 4 (A-F) shows the binding pattern of compounds **2, 3, 1, 7, 10**, and **4** respectively at the active site of COX-2. It is observed that disubstituted diazoles (compounds **1, 2, 3, 4,** and **5**) exemplify a common binding pattern while trisubstituted diazoles (compounds **6, 7, 8, 9,** and **10**) show different binding modes as compared to the binding manner of SC-558. For instance, the dinitro-carbazole and diazole groups of the disubstituted derivatives are anchored in between three binding regions; the cyclooxygenase channel (residues Y385, A527, S530), the selectivity pocket (residues H90, L352, S353, R513, F518, V523) and the common pocket (residues R120, V349, Y355, L531, L359). The substituted phenyl (or furan) ring of the disubstituted diazole derivatives is loosely accommodated at the base of the common pocket residues M113 and V116. The trisubstituted diazoles (compounds **6, 7, 8, 9,** and **10**) show two distinct binding patterns with one mode being similar orientation (compounds **6, 9,** and **10**) while the other being reversed configuration (compounds **7** and **8**) as compared to the binding mode of the disubstituted derivatives. For example, the unusual binding of trisubstituted diazoles (compounds **7** and **8**) is achieved by the interaction between the diazole moiety and the cyclooxygenase channel, the selectivity pocket, and the common pocket residues simulta-

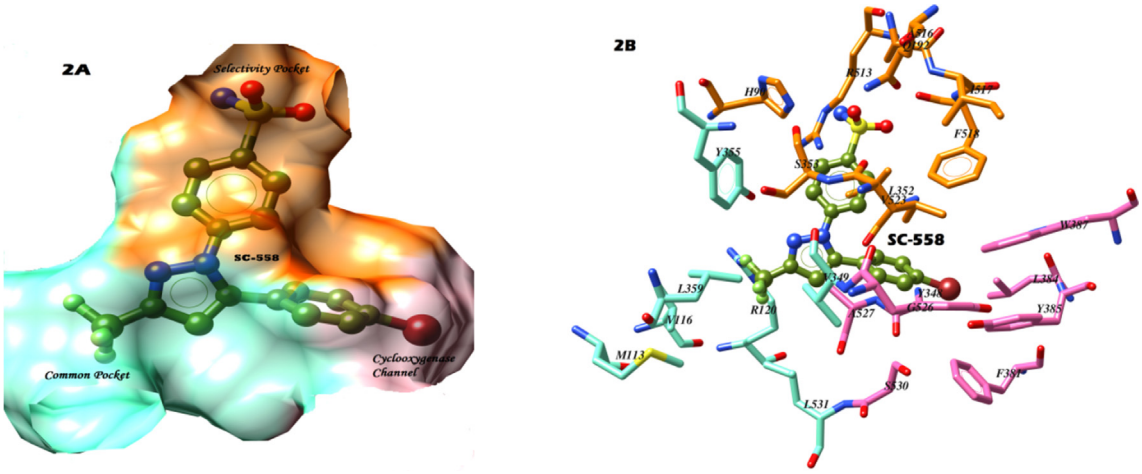

Fig. 3 The binding of SC-558 into the binding pocket of COX-2 (A) surface view of three binding regions; common pocket in cyan, cyclooxygenase channel in pink, and selectivity pocket in orange, ligand SC-558 is shown in ball and sticks. (B) Atoms and bonds view to show amino acid residues of three binding regions.

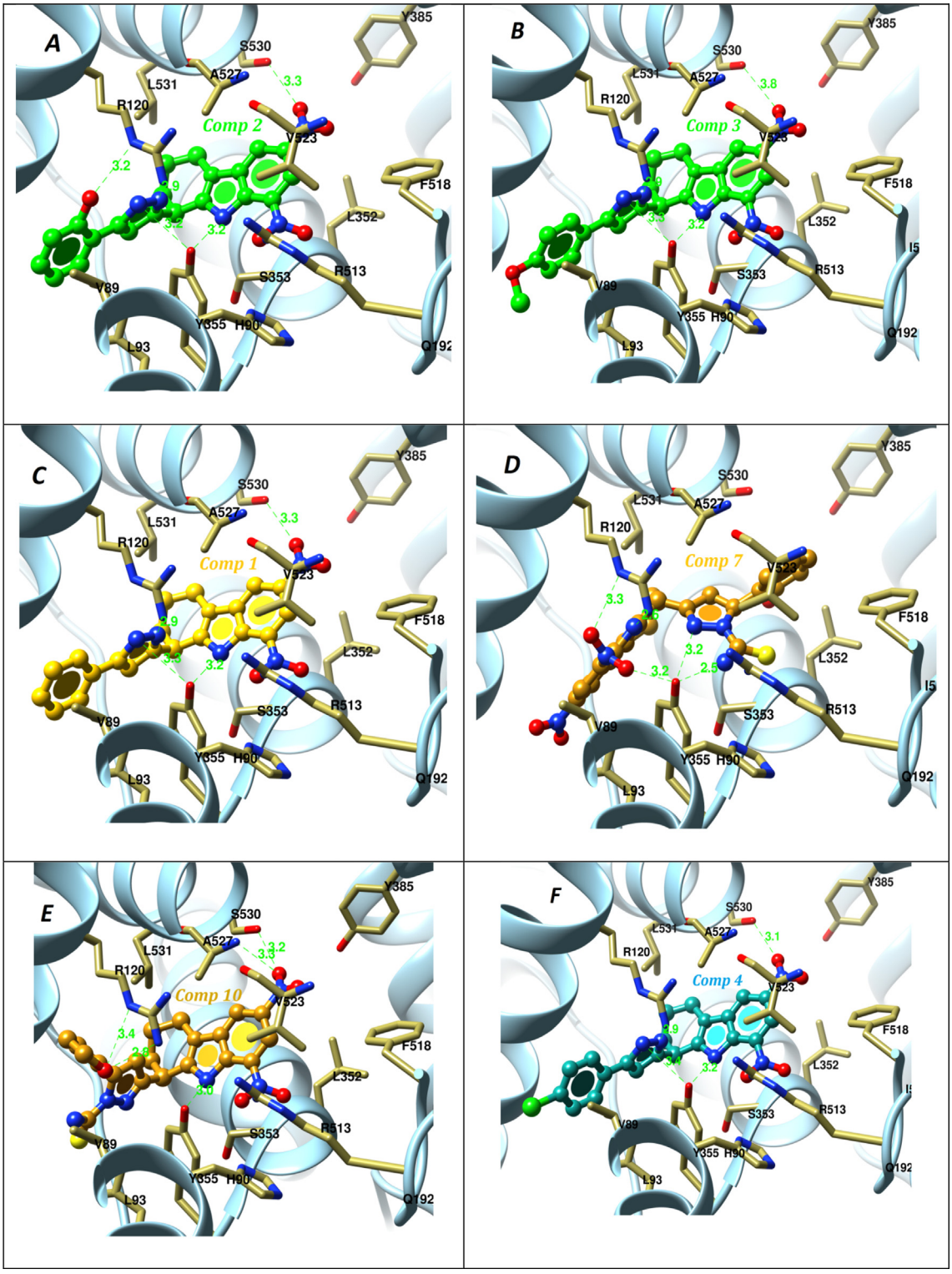

Fig. 4 The binding mode of diazole derivatives; compounds (A) 2, (B) 3, (C) 1, (D) 7, (E) 10, (F) 4 at the binding site of COX-2.

neously. Whereas the binding between the substituted phenyl ring and the cyclooxygenase channel residues, the thioamide moiety and the selectivity pocket residues, the dinitrocarbazole moiety, and the common pocket residues is observed uniquely (Fig. 4D). However, the common pattern of di- and tri-substituted analogs is observed when the dinitrocarbazole and diazole groups of the trisubstituted compounds (**6, 9,** and **10**) are occupied by the cyclooxygenase channel, the selectivity pocket and the common pocket residues simultaneously while the substituted phenyl (or furan) ring and the thioamide moiety being anchored at the base of the common pocket (Fig. 4E).

3.5.2. 5-LOX

The crystal structure of 5-LOX in complex with arachidonic acid (PDB-ID: 3V99) was utilized to investigate the binding ability of the synthesized diazoles (Gilbert et al., 2021). The binding site of arachidonic acid is comprised of mainly the hydrophobic residues L368, L373, I406, A410, L414, I415, V604, L607, and L691. The iron atom, located in the middle of the binding site, is stabilized by coordinating residues H367, H372, H550, and N554. The aromatic residue, F177 contributes to complex stabilization by interacting with the

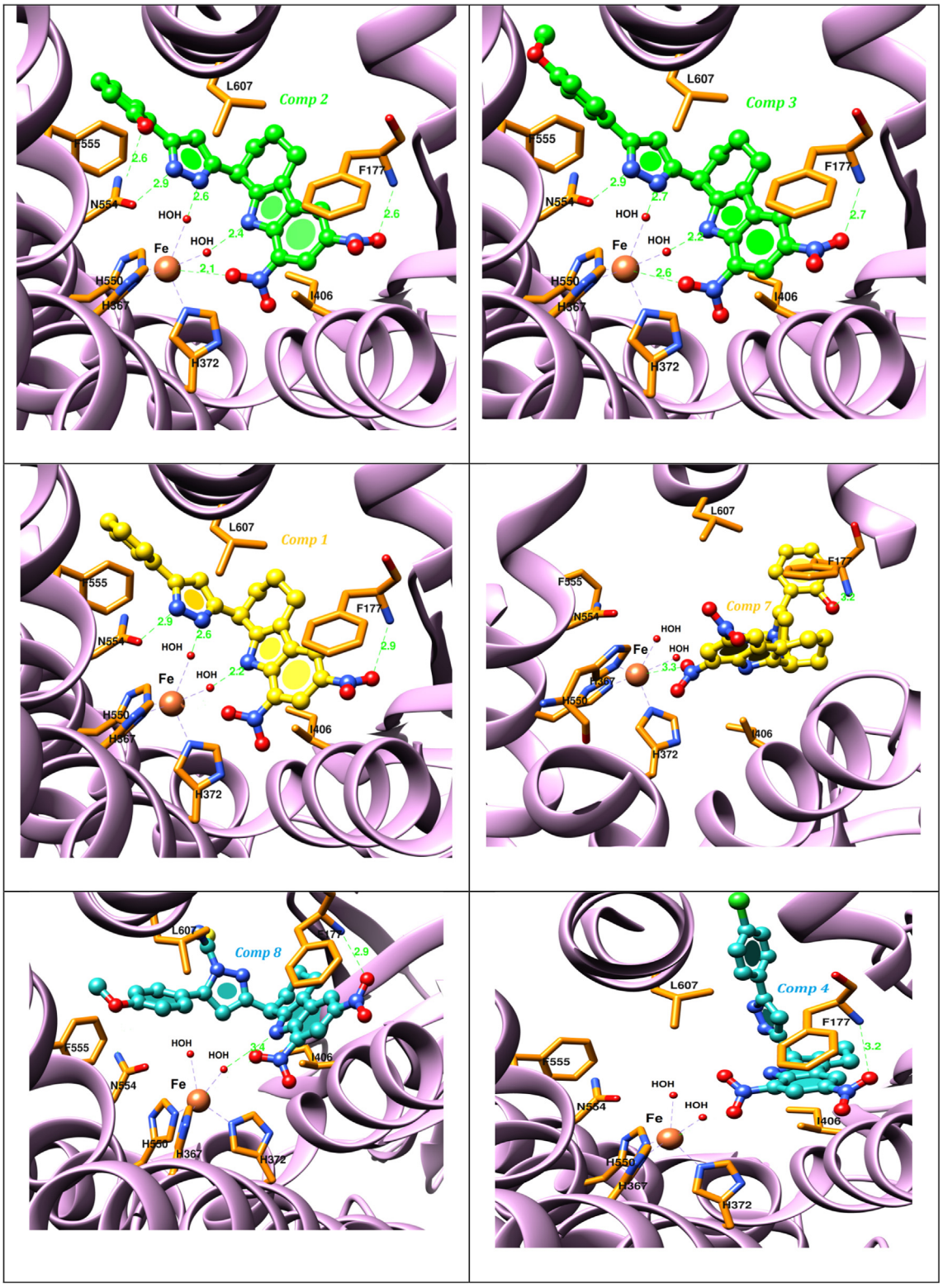

Fig. 5 The binding mode of diazole derivatives; compounds (A) 2, (B) 3, (C) 1, (D) 7, (E) 8, (F) 4 at the binding site of 5-LOX.

carboxylate moiety of arachidonic acid (Saura et al., 2016). The presence of heterocyclic rings connected by carbon chains has been observed in known 5-LOX inhibitors (Santha and Vishwanathan 2021).

Fig. 5 (A & B) displays the binding of strongly active diazoles (compounds **2** and **3**) which seems to be able to replace the third iron-bound water molecule. Compounds **2** and **3** established the coordinating distances of 2.1 Å and 2.6 Å,

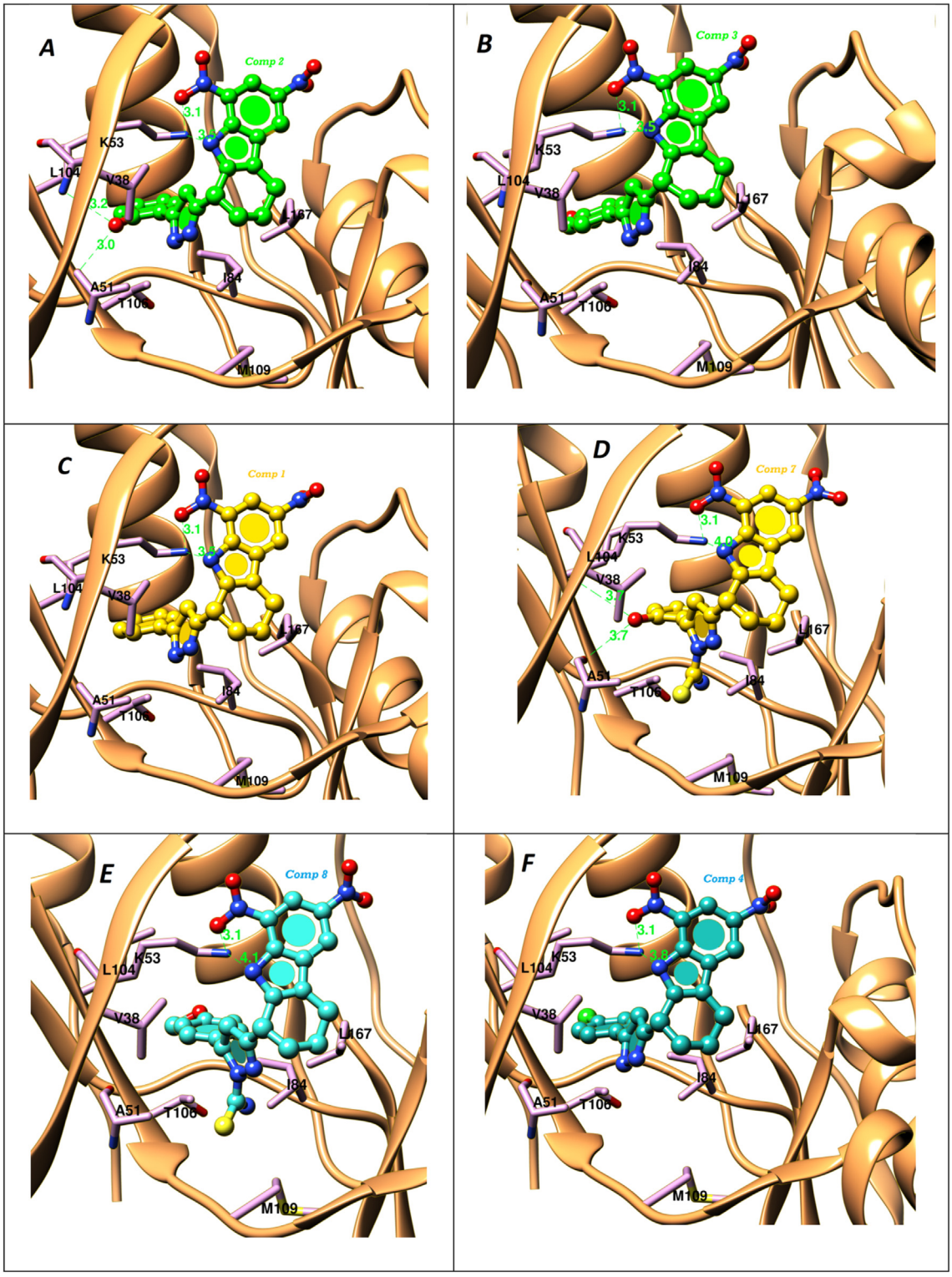

Fig. 6 Docked Pose of (A) Compound 2, (B) Compound 3, represented in light green color, (C) Compound 1, (D) Compound 7, represented as yellow color (E) Compound 8, (F), Compound 4, represented in sky blue color at the binding site of p38 α MAP Kinase. The residues V38, A51, K53, I84, L104 and T106 are shown in mauve color thin tube models.

respectively with the iron (Fe^{+2}) atom by using their oxygen atoms of the nitro substituent at ring A of the dinitrocarbazole group. However, the second nitro group at ring A of the dinitrocarbazole moiety of compounds **2** and **3** is engaged in the hydrogen bonding to the main chain nitrogen atom of the F177. The nitrogen atom presents at ring B of the dinitrocarbazole group of compounds **2** and **3** formed hydrogen bonds with the iron-bound water molecule at the distance of 2.4 and 2.2 Å, respectively. One of the nitrogen atoms of the diazole ring present in compounds **2** and **3** formed water-mediated hydrogen bonds with the iron atom at the distance of 2.6 and 2.7 Å, respectively whereas the second nitrogen atom involves the hydrogen bonding with the amidic oxygen atom of N554. One π-π interaction is observed between the substituted phenyl ring of compounds **2** and **3** and the aromatic side chain of F555 while another π-π stacking is found between the aromatic side chain of F177 and the ring A of the dinitrocarbazole group of compounds **2** and **3**. The hydrophobic residues I406 and L607 are engaged in offering the lipophilic VanderWaals contacts.

Fig. 5 (C & D) displays the binding of comparable active compounds **1** and **7**, respectively in two different modes. Compound **1** pursues the binding pattern of compounds **2** and **3** almost. For instance, compound **1** is engaged in hydrogen bonding, by using oxygen of the nitro group at ring A and the nitrogen atom at ring B of the dinitrocarbazole moiety, with the main chain nitrogen atom of F177 and the iron-bound water molecule, respectively. Similarly, both nitrogen atoms of the diazole moiety are involved in two hydrogen bonds with the oxygen atom of the iron-bound water and the amidic group of N554. Likewise, π-π interactions are also conserved by using the substituted phenyl ring and the ring A of the dinitrocarbazole group of **1** with the aromatic side chain of F555 and F177, respectively. However, compound **7** illustrates the binding pattern very differently but within the same binding site. By doing so, compound **7** abandoned numerous interactions aside from two hydrogen bonds.

Fig. 5 (E & F) reveals the docked conformation of moderately active compounds **8** and **4**, respectively in two different modes. Compound **8** pursues the binding pattern of compounds **2** and **3**, almost. For instance, **8** is engaged in the hydrogen bonding, by using the oxygen atom of the nitro group at ring A and the nitrogen atom at ring B of the dinitrocarbazole moiety, with the main chain nitrogen atom of F177 and the iron-bound water molecule, respectively. Similarly, both nitrogen atoms of the diazole moiety are involved in two hydrogen bonds with the oxygen atom of the iron-bound water and the amidic group of N554. One π-π interaction is formed between the ring A of the dinitrocarbazole group of compound **8** and the aromatic side chain of F177. However, compound **4** illustrates the binding pattern very differently but within the same binding site. By doing so, compound **4** mislaidvarious interactions apart from two hydrogen bonds.

3.5.3. MAPK p38α

The crystal structure of human p38α MAPK (PDB-ID: 4F9W) in complex with novel and selective inhibitor [N,*N*-dimethyl-6-(naphthalen-2-yl)-5-(pyridin-4-yl)pyridazin-3-amine] was used in the docking studies to rationalize the binding interaction with the synthesized diazoles (Pettersen et al., 2004). The ATP binding site of the co-crystal MAP Kinase inhibitor is recognized by a huge hydrophobic cavity containing residues V30, V38, A51, K53, L75, I84, L86, L87, L156, A157, L167, D168, L104, V105, and T106 residues. The hinge region is comprised of L108, M109, and G110 residues. The synthesized diazoles show good binding inside the ATP binding site of p38α MAP Kinase. Fig. 6 (A-F) shows the binding pattern of compounds **2, 3, 1, 7, 8**, and **4** respectively at the active site of p38α MAP Kinase. All diazole derivatives illustrate similar binding top 38α MAP Kinase in which the substituted phenyl ring and diazole moieties are anchored by hydrophobic pocket residues V38, A51, K53, I84, L104, and T106. The ring C of the dinitrocarbazole group in all diazoles is surrounded by L167. The oxygen atom of the nitro group at ring A of the dinitrocarbazole moiety of all diazole derivatives makes a hydrogen bond with the side chain nitrogen atom of K53. The nitrogen atom at ring B of the dinitrocarbazole moiety of only strongly active compounds (**2 > 3 > 1**) forms an additional hydrogen bond with the side chain nitrogen atom of K53. Table 3 demonstrates the correlation between the binding energy obtained from docking versus three anti-inflammatory therapeutic targets p38α MAPK, COX-2, 5-LOX, and IC_{50} values of the synthetic diazoles.

4. Conclusions

Highly substituted 1,2-diazoles (**1**–**10**) were prepared in excellent yield in the microwave using acid–water as the reaction medium and catalyst, previously. All synthesized compounds and standard drug, herein, were evaluated for *in vitro* anti-inflammatory activity and antioxidant potential. The disubstituted diazoles were found better than trisubstituted analogs and exhibited significant antioxidant potential. Molecular docking of diazoles showed a good correlation of their anti-inflammatory activity with p38α MAPK, COX-2, and 5-LOX enzymes that are molecular therapeutic targets of inflammation.

Declaration of Competing Interest

The authors declare that they have no known competing financial interests or personal relationships that could have appeared to influence the work reported in this paper.

References

Amir, M., Somakala, K., Ali, S., 2013. p38 MAP kinase inhibitors as anti inflammatory agents. Mini Rev. Med. Chem. 13, 2082–2096. https://doi.org/10.2174/13895575113136660098.

Anosike, C.A., Obidoa, O., Ezeanyika, L.U., 2012. Membrane stabilization as a mechanism of the anti-inflammatory activity of methanol extract of garden egg (*Solanum aethiopicum*). DARU J. Pharmac. Sci. 20, 76. https://doi.org/10.1186/2008-2231-20-76.

Ashour, S., Khateeb, M., 2011. Kinetic spectrophotometric determination of pravastatin in drug formulations via derivatization with 4-chloro-7-nitrobenzo-2-oxa-1,3-diazole (NBD-Cl). Arab. J. Chem. 4, 299–305. https://doi.org/10.1016/j.arabjc.2010.06.050.

Dewar, M.J.S., Zoebisch, E.G., Healy, E.F., et al, 1985. Development and use of quantum mechanical molecular models. 76. AM1: a new general purpose quantum mechanical molecular model. J. Am. Chem. Soc. 107, 3902–3909. https://doi.org/10.1021/ja00299a024.

Gilbert, N.C., Newcomer, M.E., Werz, O., 2021. Untangling the web of 5-lipoxygenase-derived products from a molecular and structural perspective: the battle between pro-and anti-inflammatory lipid mediators. Biochem. Pharmacol 193, 114759–11475971. https://doi.org/10.1016/j.bcp.2021.114759.

Halliwell, B., 2007. Dietary polyphenols: good, bad, or indifferent for your health? Cardiovasc. Res. 73, 341–347. https://doi.org/10.1016/j.cardiores.2006.10.004.

Karrat, L., Abajy, M.Y., Nayal, R., 2022. Investigating the anti-inflammatory and analgesic properties of leaves ethanolic extracts of Cedrus libani and Pinus brutia. Heliyon 8 (4). https://doi.org/10.1016/j.heliyon.2022.e09254.

Konturek, P.C., Kania, J., Burnat, G., et al, 2005. Prostaglandins as mediators of COX-2 derived carcinogenesis in gastrointestinal tract. J. Physiol. Pharmacol. 56 (Suppl 5), 57–73.

Kostopoulou, I., Diassakou, A., Kavetsou, E., et al, 2021. Novel quinolinone–pyrazoline hybrids: synthesis and evaluation of antioxidant and lipoxygenase inhibitory activity. Mol. Divers 25, 723–740. https://doi.org/10.1007/s11030-020-10045-x.

Kumar, V., Bhat, Z.A., Kumar, D., et al, 2011. In-vitro anti-inflammatory activity of leaf extracts of *Basella alba* Linn. var. *alba*. Int. J. Drug Dev. Res. 3, 176–179.

Kumar, S., Boehm, J., Lee, J.C., 2003. p38 MAP kinases: key signalling molecules as therapeutic targets for inflammatory diseases. Nat. Rev. Drug Discov. 2, 717–726. https://doi.org/10.1038/nrd1177.

Kurumbail, R.G., Stevens, A.M., Gierse, J.K., et al, 1996. Structural basis for selective inhibition of cyclooxygenase-2 by anti-inflammatory agents. Nature 384, 644–648. https://doi.org/10.1038/384644a0.

Limongelli, V., Bonomi, M., Marinelli, L., et al, 2010. Molecular basis of cyclooxygenase enzymes (COXs) selective inhibition. PNAS 107, 5411–5416. https://doi.org/10.1073/pnas.0913377107.

Liu, C., Wrobleski, S.T., Lin, J., et al, 2005. 5-Cyanopyrimidine derivatives as a novel class of potent, selective, and orally active inhibitors of p38alpha MAP kinase. J. Med. Chem. 48, 6261–6270. https://doi.org/10.1021/jm0503594.

Lugasi, A., 1997. Natural Antioxidants Chemistry, Health Effects, and Applications. Edited by F. Shahidi. VIII and 432 pages, numerous figures and tables. AOCS Press, Champaign, Illinois, 1997. Food/Nahrung. 41, 321. https://doi.org/10.1002/food.19970410536.

Mehmood, R., Sadiq, A., Alsantali, R.I., Mughal, E.U., Alsharif, M. A., Naeem, N., Javid, A., Al-Rooqi, M.M., Chaudhry, G.E., Ahmed, S.A., 2022. Synthesis and evaluation of 1,3,5-triaryl-2-pyrazoline derivatives as potent dual inhibitors of urease and α-glucosidase together with their cytotoxic, molecular modeling and drug-likeness studies. ACS Omega 7 (4), 3775–3795. https://doi.org/10.1021/acsomega.1c06694.

Morris, G.M., Goodsell, D.S., Halliday, R.S., et al, 1998. Automated docking using a Lamarckian genetic algorithm and an empirical binding free energy function. J. Comput. Chem. 19, 1639–1662. https://doi.org/10.1002/(SICI)1096-987X(19981115)19:14<1639::AID-JCC10>3.0.CO;2-B.

Natarajan, S.R., Liu, L., Levorse, M., et al, 2006. p38 MAP kinase inhibitors. Part 5: discovery of an orally bio-available and highly efficacious compound based on the 7-amino-naphthyridone scaffold. Bioorg. Med. Chem. Lett. 16, 5468–5471. https://doi.org/10.1016/j.bmcl.2006.06.084.

Nieminen, R., Leinonen, S., Lahti, A., et al, 2005. Inhibitors of mitogen-activated protein kinases downregulate COX-2 expression in human chondrocytes. Mediators Inflamm. 2005, 249–255. https://doi.org/10.1155/mi.2005.249.

Oyedapo, O.O., Famurewa, A.J., 1995. Antiprotease and membrane stabilizing activities of extracts of *Fagera zanthoxycoides*, *Olax subscorpiodes* and *Tetra plenra tetraptera*. Int. J. Pharmacognosy. 33, 65–69.

Parke, D.V., 1991. Free radicals in biology and medicine (second ed.). FEBS Lett. 284, 135–136. https://doi.org/10.1016/0014-5793(91)80785-2.

Pettersen, E.F., Goddard, T.D., Huang, C.C., et al, 2004. UCSF Chimera–a visualization system for exploratory research and analysis. J. Comput. Chem. 25, 1605–1612. https://doi.org/10.1002/jcc.20084.

Prasad, S., Kulshreshtha, A., Lall, R., Gupta, S.C., 2021. Inflammation and ROS in arthritis: management by Ayurvedic medicinal plants. Food Funct. 12 (18), 8227–8247.

Prieto, P., Pineda, M., Aguilar, M., 1999. Spectrophotometric quantitation of antioxidant capacity through the formation of a phosphomolybdenum complex: specific application to the determination of vitamin E. Anal. Biochem. 269, 337–341. https://doi.org/10.1006/abio.1999.4019.

Re, R., Pellegrini, N., Proteggente, A., et al, 1999. Antioxidant activity applying an improved ABTS radical cation decolorization assay. Free Radic. Biol. Med. 26, 1231–1237. https://doi.org/10.1016/s0891-5849(98)00315-3.

Revesz, L., Blum, E., Di Padova, F.E., et al, 2004. Novel p38 inhibitors with potent oral efficacy in several models of rheumatoid arthritis. Bioorg. Med. Chem. Lett. 14, 3595–3599. https://doi.org/10.1016/j.bmcl.2004.03.106.

Sadiq, Z., Hussain, E.A., Naz, N., et al, 2017. Microwave-assisted synthesis of tetrahydrocarbazole linked 1,2-diazoles in aqueous-Brønsted acid catalytic system. J. Chem. 2017, 3902751. https://doi.org/10.1155/2017/3902751.

Saklatvala, J., 2004. The p38 MAP kinase pathway as a therapeutic target in inflammatory disease. Curr. Opin. Pharmacol. 4, 372–377. https://doi.org/10.1016/j.coph.2004.03.009.

Santha, S.S.R., Vishwanathan, A.S., 2021. Mechanistic insights into 5-lipoxygenase inhibition by pyocyanin: a molecular docking and molecular dynamics study. J. Biomol. Struct. Dyn. 25, 1–9. https://doi.org/10.1080/07391102.2021.1934543.

Saura, P., Maréchal, J.D., Masgrau, L., et al, 2016. Computational insight into the catalytic implication of head/tail-first orientation of arachidonic acid in human 5-lipoxygenase: consequences for the positional specificity of oxygenation. PCCP 18, 23017–23035. https://doi.org/10.1039/c6cp03973a.

Schieven, G.L., 2005. The biology of p38 kinase: a central role in inflammation. Curr. Top. Med. Chem. 5, 921–928. https://doi.org/10.2174/1568026054985902.

Sherin, L., Mustafa, M., Shujaat, S., 2015. Evaluation of *Terminalia bellerica* Roxb. leaf extracted in different solvents for antioxidant activities. Asian J. Chem. 27, 4527–4531. https://doi.org/10.14233/ajchem.2015.19208.

Thompson, M.A., 2004. Molecular docking using ArgusLab, an efficient shape-based search algorithm and the AScore scoring function. In: Proceedings of the ACS Meeting, Philadelphia, Pa, USA.

Thach, L., Riewe, S., Camillo, A., 2021. Generational cohort theory and wine: analyzing how gen Z differs from other American wine consuming generations. Int. J. Wine Bus. Res. 33 (1), 1–27. https://doi.org/10.1108/IJWBR-12-2019-0061.

Trott, O., Olson, A.J., 2010. AutoDock Vina: improving the speed and accuracy of docking with a new scoring function, efficient optimization, and multithreading. J. Comput. Chem. 31, 455–461. https://doi.org/10.1002/jcc.21334.

Watterson, D.M., Grum-Tokars, V.L., Roy, S.M., et al, 2013. Development of novel in vivo chemical probes to address CNS protein kinase involvement in synaptic dysfunction. PloS One 8, e66226.

Williams, C.S., DuBois, R.N., 1996. Prostaglandin endoperoxide synthase: why two isoforms? Am. J. Physiol. 270, G393–G400. https://doi.org/10.1152/ajpgi.1996.270.3.G393.

Wu, Y., He, C., Gao, Y., et al, 2012. Dynamic modeling of human 5-lipoxygenase-inhibitor interactions helps to discover novel inhibitors. J. Med. Chem. 55, 2597–2605. https://doi.org/10.1021/jm201497k.